Systematic Design and Circuit Analysis of Lightning Impulse Voltage Generation on Low-Inductance Loads

Peerawut Yutthagowith *, Phattarin Kitcharoen and Anantawat Kunakorn

School of Engineering, King Mongkut's Institute of Technology Ladkrabang, 1 Chalongkrung Rd., Ladkrabang, Bangkok 10520, Thailand; phattarin.ki@gmail.com (P.K.); anantawat.ku@kmitl.ac.th (A.K.)
* Correspondence: peerawut.yu@kmitl.ac.th; Tel.: +66-(0)-2-329-8330

Abstract: The well-known circuit for the generation of lightning impulse voltage (LIV) on low-inductance loads was introduced by Glaninger in 1975, and the circuit component selection was proposed by Feser. However, the circuit and the approach for the component selection have some difficulties for which further adjustment is required for obtaining the waveform parameters according to the standard requirement. In this paper, an extended Glaninger's circuit with an additional series resistor is proposed. Furthermore, a systematic design and circuit analysis of LIV generation for low-inductance loads are developed. With the help of a circuit simulator, the circuit analysis for the component selection is described. The validity of the proposed circuit was confirmed by some experimental results in comparison with the simulated ones. The proposed circuit and component selection provide not only the generation waveform according to the standard requirement but also other promising performances in terms of the wide inductance load range from 400 µH to 4 mH, a voltage efficiency of over 80%, an overshoot voltage of below 5%, an undershoot voltage of below 40%, and a maximum charging capacitance of 10 µF. From the simulated and experimental results, the proposed circuit and component selection approach is very useful for the LIV tests on low-inductance loads instead of using the conventional approach based on trial and error.

Keywords: circuit design; Glaninger's circuit; high-voltage tests; lightning impulse voltages; low-inductance load; reactor; transformer windings

1. Introduction

Reactors and transformers are crucial equipment in high-voltage (HV) power systems. It is necessary to confirm the insulation performance of such equipment before its installation in the actual systems. The lightning impulse voltage (LIV) test is employed for investigation of the transient insulation performance of the HV equipment. A simple resistor–capacitor circuit named Marx's circuit [1] as shown in Figure 1 is utilized for the generation of the LIV on the equipment undergoing tests. The circuit is composed of a charging capacitor (C_s), a front-time resistor (R_d), a tail-time resistor (R_e), and a load in the form of a capacitor (C_b).

According to international standards [2,3], the full LIV waveform parameters and their tolerances are defined by the front-time (T_1 = 1.2 µs ± 30%), the time to half (T_2 = 50 µs ± 20%), and the peak voltage (V_p). In the case of a simple load represented by a capacitor, the adjustment of the time and peak voltage parameters can be performed by adjusting R_d and R_e in accordance with Equations (1) and (2), and the charging voltage of the charging capacitor, respectively.

$$T_1 = 2.96 R_d \frac{C_b C_s}{C_b + C_s} \tag{1}$$

$$T_2 = 0.73 R_e (C_b + C_s) \tag{2}$$

(**a**)

(**b**)
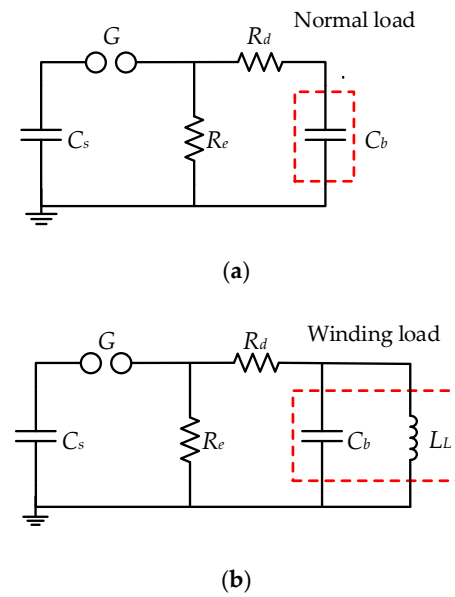
Figure 1. Conventional Marx's circuits with normal and winding loads for generation of impulse voltage. (**a**) Normal load, (**b**) Winding load.

In the cases of tests on winding loads, an overshoot rate of no greater than 5% is necessary for control according to the standard requirement [4,5]. However, the equivalent circuits of some loads, such as medium-voltage, low-voltage, and air-core reactor windings, cannot be represented well by only a capacitor. The proper equivalent circuit should be an inductor and a capacitor in parallel connection as shown in Figure 1b, otherwise, it causes the conventional circuit generating the distort the LIV waveform from the standard requirement [4–9]. There are some studies [10–12] utilizing rigorous approaches for adjusting the waveform parameters according to the standard requirements. A crucial problem is that it is very hard to adjust the circuit components to obtain T_2 longer than 40 µs, even though a charging capacitance (C_s) of over 10 µF, and a very high tail-time resistance (R_e) of over 1 MΩ, are employed in the generation circuit. For a better understanding, Test Cases 1 and 2 should be considered. In these cases, the circuit parameters of the equivalent circuit of the load, including a measuring system, are given in Table 1. The winding inductance and capacitance of the system are 2 mH and 4 nF, respectively. The simulated waveforms of the considered cases are shown in Figure 2. The times for half of Test Cases 1 and 2 are 12.16 µs and 15.53 µs, respectively. From the simulated results, it confirms that an increase in C_s and R_e is not an effective way to obtain the waveform according to the standard requirement.
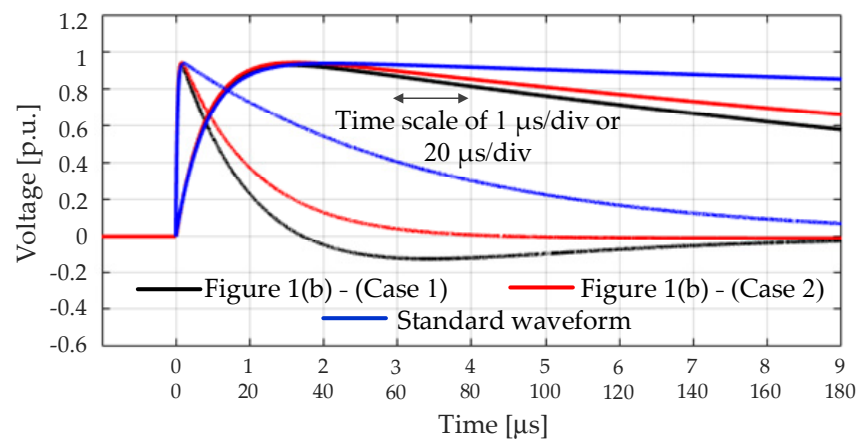
Figure 2. Waveforms generated by the conventional circuit in comparison with the standard lightning impulse voltage waveform.

Table 1. Circuit component parameters used for lightning impulse voltage generation and waveform parameters of the generated waveforms.

Circuit Type — Circuit and Time Parameters	Figure 1b (Case 1)	Figure 1b (Case 2)	Figure 3 (Case 3 and K. Feser)	Figure 3 (Case 4 and this Paper)
L_L	2.0 mH	2.0 mH	2.0 mH	2.0 mH
C_b	4.0 nF	4.0 nF	4.0 nF	4.0 nF
C_s	2.0 μF	20.0 μF	2.0 μF	2.0 μF
R_d	100 Ω	100 Ω	100 Ω	100 Ω
L_d	-	-	125 μH	200 μH
R_p	-	-	1600 Ω	500 Ω
R_e	45 Ω	∞ Ω	52 Ω	50 Ω
Voltage Efficiency	92.63%	93.99%	105.98%	93.45%
Overshoot rate (<5%)	−0.69% (✓)	−0.40% (✓)	+8.11% (✗)	+0.17% (✓)
Undershoot rate (<50%)	13.3% (✓)	6.12% (✓)	37.0% (✓)	38.4% (✓)
T_1 (0.84 μs–1.56 μs)	1.05 μs (✓)	1.08 μs (✓)	0.985 μs (✓)	1.07 μs (✓)
T_2 (40 μs–60 μs)	12.16 μs (✗)	15.53 μs (✗)	36.97 μs (✗)	40.4 μs (✓)

✓ is indicated for the parameters in accordance with the standard requirement. ✗ is indicated for the parameters not in accordance with the standard requirement.

To overcome the problem of the waveform adjustment using the conventional generation circuit, Glaninger's circuit, as shown in Figure 3, was proposed in 1975 [8], and the circuit component selection was proposed by Feser [13]. The additional inductor and resistor (L_d and R_p) are connected to the circuit. The components can be selected by Equations (3)–(6).
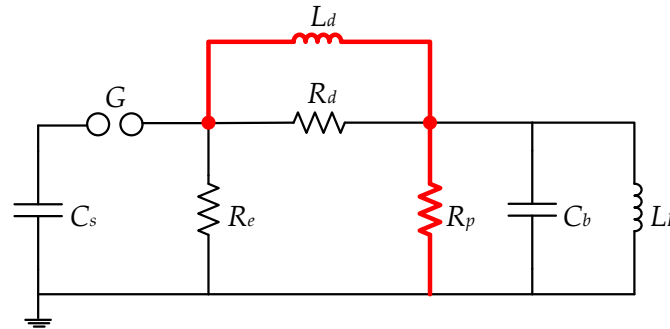
Figure 3. Glaninger's circuit with a winding load.

$$C_s \approx T_2^2 / L_L \tag{3}$$

$$R_d = 0.4 \times 10^{-6} C_b \tag{4}$$

$$L_d = 1.25 \times 10^{-6} R_d \tag{5}$$

$$R_p = (R_d L_L) / L_d \tag{6}$$

L_d is used for bypassing the current at the low-frequency range, or after the time to peak voltage. It leads to the waveform having the longer T_2. R_p is employed for controlling the overshoot rate. R_e is also utilized for controlling the undershoot voltage which should be less than 50%. However, it is found that for obtaining the waveform according to the standard requirement, the circuit components selected by Feser's approach still require further adjustment.

For a better understanding, LIV generation on the load of which the equivalent circuit is a 2 mH inductor and a 4 nF capacitor in parallel connection (the same load in Figure 2) should be considered. Glaninger's circuit and Feser's component selection were employed to generate LIV. The selected circuit components in Case 3 are given in Table 1. It is found that the generated waveform, as shown in Figure 4, is deviated from the standard requirement. The voltage efficiency (the ratio of the generated peak voltage to the charging voltage), the overshoot rate, and T_2 are 105.98%, +8.11% ($\geq$5%), and 36.97 µs ($\leq$36.97 µs), respectively. It is noted that due to unavoidable parasitic inductance and the additional inductance, the generation circuit becomes an RLC circuit. The switch to an RLC circuit can generate an overvoltage, of which the peak is over 100% of the charging voltage. The waveform does not accord with the standard requirement. Therefore, further adjustment is required for obtaining the proper waveform. The adjusted circuit components in Case 4 are also given in Table 1. It is noted that the adjusted circuit components agree with the results calculated by the proposed method, which will be explained in the next section. As shown in Figure 4, the waveform parameters, i.e., T_1 of 1.07 µs, T_2 of 40.4 µs, the overshoot rate of +0.17%, and the undershoot rate of +38.4%, accord with the standard requirement.
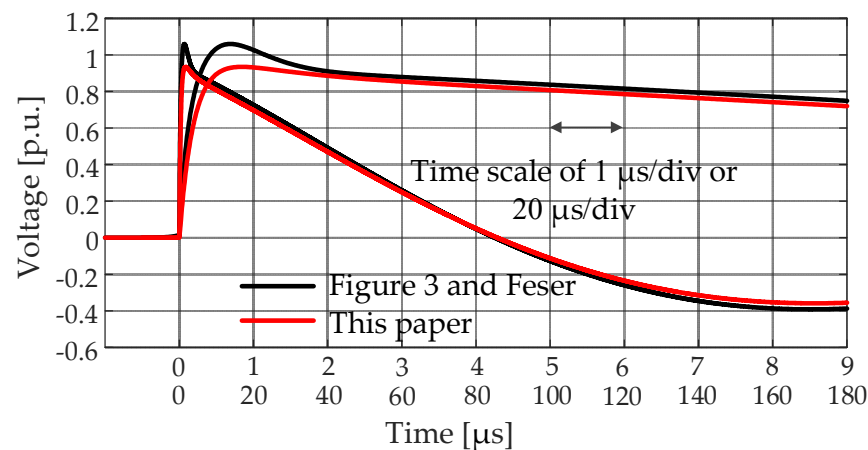
Figure 4. Comparison of waveforms generated by Glaninger's circuits.

The complex approach based on neural networks for waveform adjustment was proposed in [10], but physical meaning is lost in the approach. In this paper, based on circuit analysis, the effectiveness of the simple approach is proposed. However, in our best knowledge, there is no simple and comprehensive approach for waveform adjustment in Glaninger's circuit. Most test engineers are still using their own experience in the process of waveform adjustment. Because of this, it will be advantageous if an effective LIV generation circuit and a systematic approach for circuit component selection are developed. In this paper, an extended Glaninger's circuit with an additional series resistor is proposed. Furthermore, a systematic design and circuit analysis of lightning impulse voltage (LIV) generation for low-inductance loads are developed and described. The validity of the proposed circuit was confirmed by experimental results in comparison with simulated results. The proposed circuit and component selection provide not only the generated waveform according to the standard requirement, but also additional promising performances in terms of the wide inductance load range, from 400 µH to 4 mH, a voltage efficiency of over 80%, an overshoot voltage of below 5%, an undershoot voltage of below 40%, and a maximum charging capacitance of 10 µF. From the simulated and experimental results, the validity of the proposed circuit and component selection approach confirms that it is very useful for LIV tests on low-inductance loads compared to using the conventional approach based on trial and error.

2. Circuit Analysis and Component Selection of the LIV Generation for Low-Inductance Loads

A circuit of full lightning impulse voltage generation on a low-inductance load is proposed and analyzed. The circuit is the extension of the Glaninger's circuit, as shown in Figure 5. The effective range of the inductance load of the proposed circuit is from 0.4 mH to 4 mH [13,14].
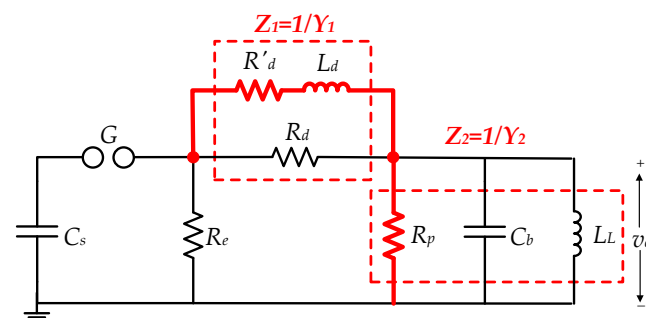
Figure 5. The proposed circuit for LIV generation for low-inductance loads.

From the equivalent circuit in Figure 5, a differential equation can be derived in order to determine the output (v_o). This differential equation is in the form of the fourth-order ordinary equation, as shown in Equation (7), where P, Q, R, and S are coefficients of the differential equation. The possible solutions of the characteristic equation of Equation (7) are categorized into three cases. The first one is composed of four real root numbers. The second one is composed of two real root numbers, and a complex conjugate pair. The third one is composed of two complex number pairs. The possible solutions in the time domain are given as Equation (8). Due to the low-inductance load, the possible solutions can only be the second and third cases.

$$\frac{d^4 v_o}{dt^4} + P\frac{d^3 v_o}{dt^3} + Q\frac{d^2 v_o}{dt^2} + R\frac{dv_o}{dt} + Sv_o = 0 \tag{7}$$

$$v_o(t) = \begin{cases} A_1 e^{-\alpha_1 t} + A_2 e^{-\alpha_2 t} + A_3 e^{-\alpha_3 t} + A_4 e^{-\alpha_4 t} \\ A_1 e^{-\alpha_1 t} + A_2 e^{-\alpha_2 t} + A_3 e^{-\alpha_3 t} sin(\omega_1 t + \phi_1) \\ A_1 e^{-\alpha_1 t} sin(\omega_1 t + \phi_1) + A_2 e^{-\alpha_2 t} sin(\omega_2 t + \phi_2) \end{cases} \tag{8}$$

The proposed circuit operates in a similar manner to Glaninger's circuit. There are two operation modes, i.e., a charging mode during the front part of the waveform and a discharging mode during the tail part of the waveform. The simplified circuits during such modes are shown in Figure 6.
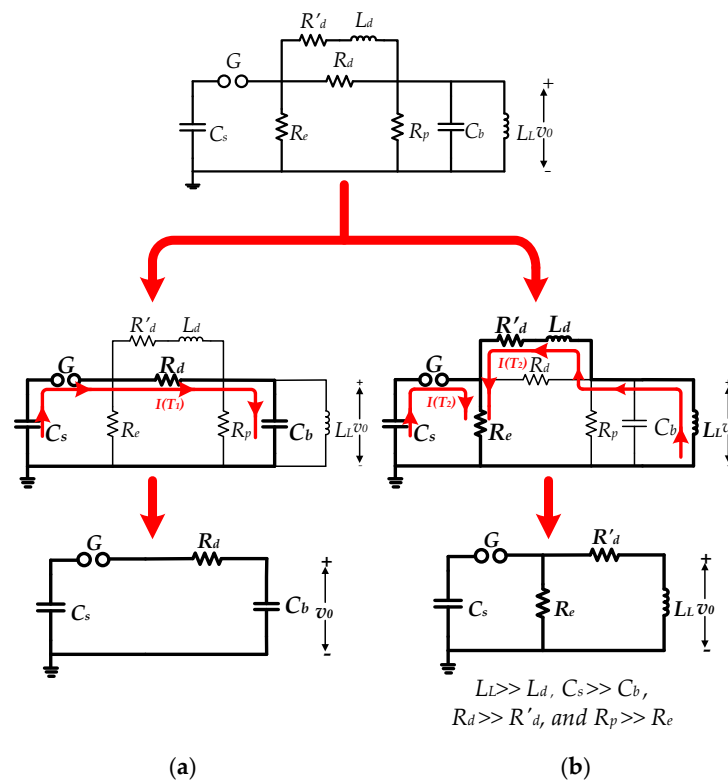
Figure 6. The equivalent circuits during charging and discharging modes of the lightning impulse voltage generation. (**a**) Charging mode, (**b**) Discharging mode.

In the charging mode during the front part of the waveform, the equivalent circuit in Figure 6a is considered. The additional inductor (L_d), and the load inductor (L_L), act with high impedance due to a high rate of voltage change or a high-frequency range. The load capacitor (C_b) is charged up by the charging current from the charging capacitor (C_s), and the voltage across the test object is raised to the impulse peak voltage. At the discharging mode during the tail part of the waveform, the equivalent circuit in Figure 6b is considered. The additional inductor (L_d) and the load inductor (L_L) act as a low impedance

due to low rate of voltage change or a low-frequency range. The load capacitor (C_b) is connected with the charging capacitor (C_s) through the additional inductor (L_d) and the additional series resistor (R'_d). The front-time resistor has no effect on the discharging mode operation. At the discharging mode, two currents form the charging capacitor and the load capacitor flow through the tail-time and additional parallel resistors during the tail part of the generated waveform. Please note that the additional series resistor (R'_d) should be much smaller than the front-time resistor (R_d) in the proposed circuit. The voltage across the load oscillates with the resonant frequency due to the total inductance ($L_d + L_L$) and the charging capacitance (C_s). For avoiding waveform distortion, i.e., the oscillation and overshoot on the peak of the waveform, R_p has to be selected properly. Additionally, for damping the undershoot caused by the oscillation due to the total inductance ($L_d + L_L$) and C_s, the appropriate additional series resistance (R'_d), and the tail-time resistance (R_e), have to be designed properly. From the explanation of the circuit operation, the appropriate circuit parameters can be selected by the following procedure.

In the first step, the load inductance (L_L) and the load capacitance (C_b) are necessarily given and measured. At the charging mode, the front-time resistance can be calculated by Equation (1), and on the assumption of $C_s \gg C_b$, Equation (1) is simplified by Equation (9).

$$R_d = \frac{0.405 \times 10^{-6}}{C_b} \tag{9}$$

In the second step, during the discharging mode, the voltage across the load is oscillated by the resonant frequency (f_r) approximated by Equation (10), and the time period (T) is approximated by Equation (11).

$$f_r \approx \frac{1}{2\pi\sqrt{(L_d + L_L)C_s}} \approx \frac{1}{2\pi\sqrt{L_L C_s}}; \ L_d \ll L_L \tag{10}$$

$$T \approx 2\pi\sqrt{L_L C_s} \tag{11}$$

For controlling the time to half of the generated waveform, one-tenth of the time period is supposed to be greater than the minimum time to half (40 µs), as expressed in Equation (12). Then, the charging capacitance (C_s) can be approximated from rewriting Equation (12) as expressed in Equation (13).

$$\frac{T}{10} \geq 40 \times 10^{-6} \tag{12}$$

$$C_s \geq \frac{\left(\frac{400 \times 10^{-6}}{2\pi}\right)^2}{L_L} = \frac{4.053 \times 10^{-9}}{L_L} \tag{13}$$

In the third step, the additional inductance acts with low impedance at the charging mode. The impedance of the inductor should be much less than the front-time resistor at the front-time period or at the dominant frequency (f_d) of about 250 kHz. Additionally, in the discharging mode, the impedance of the inductor should be much greater than the front-time resistor at the tail-time period or at the resonant frequency (f_r). To elaborate, the impedance range is shown in Equations (14) and (15), and the additional inductance (L_d) can be approximated from rewriting Equations (14) and (15) as expressed in Equation (16).

$$2\pi f_d L_d \geq R_d \tag{14}$$

$$2\pi f_r L_d \leq R_d \tag{15}$$

$$\frac{R_d}{2\pi f_d} \leq L_d \leq R_d\sqrt{L_L C_s} \tag{16}$$

Even through an inductor with the required inductance can be made in a testing laboratory, for convenience, in the lightning impulse voltage tests, inductors with inductances of 50 μH, 100 μH, 200 μH, and 400 μH are recommended to construct and use.

In the fourth step, for controlling the distortion of the generated waveform, the overshoot and the oscillation on the waveform must be minimized by selectinga proper additional parallel resistance (R_p). Such waveform distortion is caused by the differences in the voltage divisions between the load impedance (Z_1) and total impedance ($Z_1 + Z_2$) at the low frequency and at the resonant frequency. Therefore, the ratio of the load impedance (Z_1) to the total impedance ($Z_1 + Z_2$) at the low frequency must be equal to this ratio at the resonant frequency. However, it is acceptable for an overshoot rate of less than 5%. The overshoot factor (k_p) is applied to adjust the overshoot rate in Equations (17) and (18), calculating the appropriate additional parallel resistance (R_p). An appropriate overshoot factor is in the range from 0.95 to 1.05.

$$k_p \left(\frac{L_L}{L_L + L_d} \right) = \left| \frac{Z_1}{Z_1 + Z_2} \right| = \left| \frac{Y_2}{Y_1 + Y_2} \right| \tag{17}$$

$$k_P^2 \left(\frac{L_L}{L_L + L_d} \right)^2 = \frac{\left(\frac{1}{R_d} \right)^2 + \left(\frac{1}{\omega_r L_d} \right)^2}{\left(\frac{1}{R_d} + \frac{1}{R_p} \right)^2 + \left(\omega_r C_b - \frac{1}{\omega_r L_L} - \frac{1}{\omega_r L_d} \right)^2}; \ \omega_r = 2\pi f_r \tag{18}$$

For a better understanding, example cases should be considered for demonstration of the effect of the overshoot factor (k_p). The load equivalent circuit is simply represented by a 2 mH inductor connected in parallel with a 4 nF load capacitor. The circuit parameters of the generation circuit were selected by the proposed approach. With the various additional parallel resistances (R_p) associated with the overshoot factors, the ratios between the load impedance (Z_1) and the total impedance ($Z_1 + Z_2$) are plotted in the frequency domain, as shown in Figure 7. Furthermore, the voltages across the load are plotted in the time domain, as shown in Figure 8. It is found that the appropriate overshoot factor is in the range from 0.95 to 1.05 without an acceptable distortion in an impulse voltage waveform. The selection of an overshoot factor higher than 1.05 provides better voltage efficiency. However, this leads to an overshoot rate over 5%.
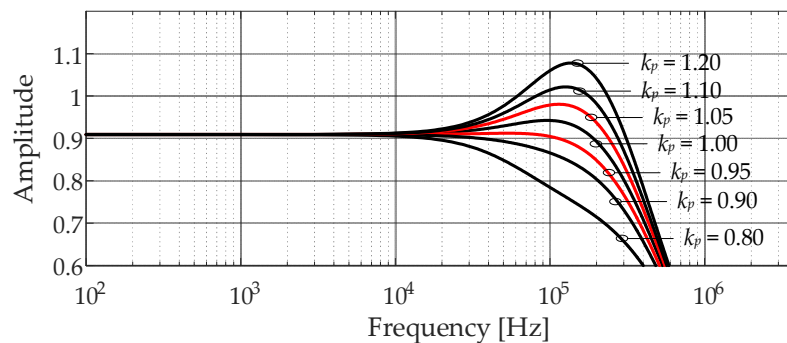
Figure 7. Comparison of the overshoot factor effects in the frequency domain.

(a)

(b)
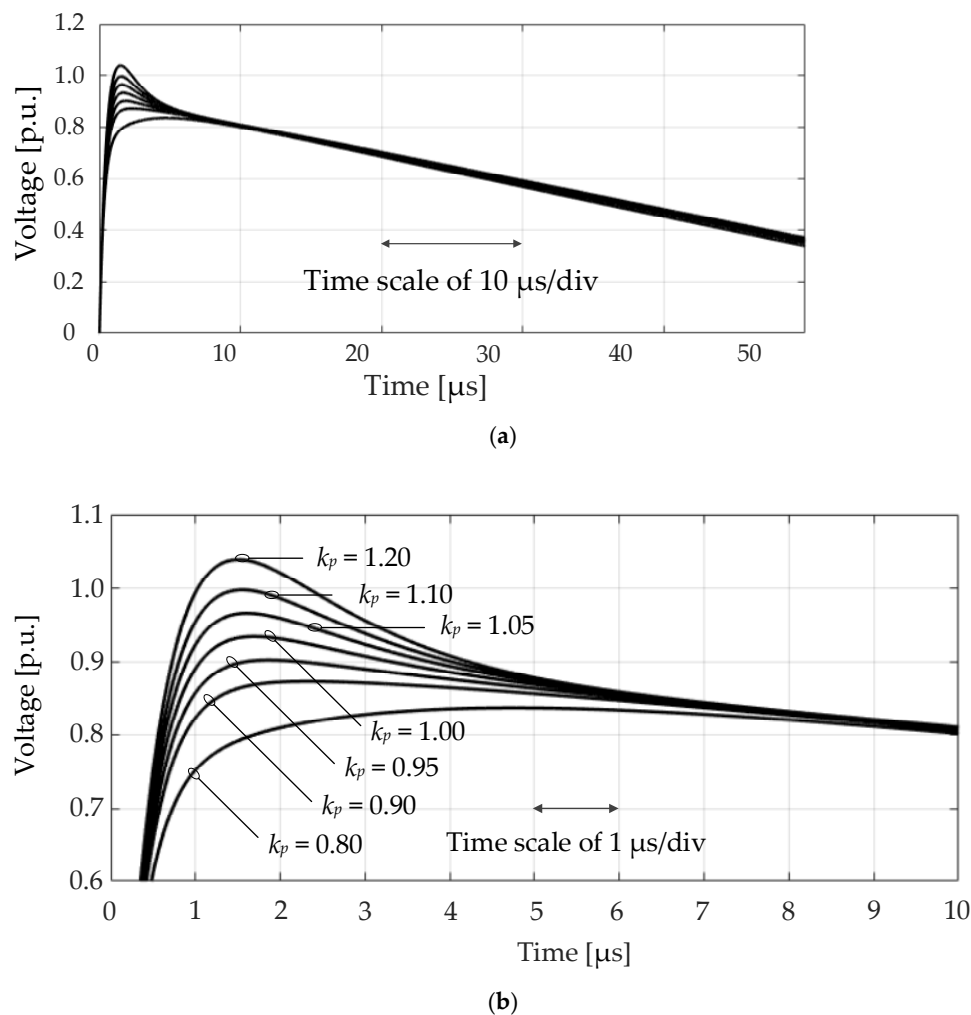
Figure 8. Comparison of the overshoot factor effects on the generated waveforms in the time domain. (**a**) Long span time scale, (**b**) Short span time scale.

In the final step, to obtain a waveform undershoot of less than 50%, the additional series and tail-time resistances (R'_d and R_e) act as a dissipation loss in the generated circuit during the discharging mode operation. Under such an operation mode, the waveform on the tail part is only considered. Based on assumption of $C_s \gg C_b$, $R_p \gg R_e$, $R_d \gg R'_d$, and $L_L \gg L_d$, the equivalent circuit of the proposed circuit in Figure 5 can be simplified, as shown in Figure 6b.

The solution of the simplified circuit becomes the second-order ordinary differential equation, as given in Equation (19).

$$\frac{d^2 v_o}{dt^2} + 2\zeta\omega\frac{dv_o}{dt} + \omega_0^2 v_o = 0 \tag{19}$$

where, ω_0 is a natural angular frequency and ζ is the damping factor. The definitions of those parameters are expressed in Equations (20) and (21).

$$\omega_0 = \sqrt{\frac{R_d + R_e}{L_L C_s R_e}} \tag{20}$$

$$\zeta = \left(\frac{R_d}{L_L} + \frac{1}{C_s R_e}\right)\sqrt{\frac{L_L C_s R_e}{R_d + R_e}} \tag{21}$$

Due to the low-inductance load, the solution of Equation (19) will be the underdamped condition, and can be expressed in Equation (22).

$$v_o(t) = V_{ch}e^{-\zeta\omega_0 t} \cos\left(\omega_0\sqrt{1-\zeta^2}t\right) \tag{22}$$

From Equation (22), the undershoot rate is dependent on the damping factor. By varying the damping factor (ζ), the relation of the damping factor and the undershoot rate (γ) can be found. Increasing the damping factor affects a decrease in the undershoot rate. With a curve fitting method, the percentage of the undershoot rate can be approximated in the function of the damping factor, as given in Equation (23).

$$\zeta = f(\gamma) \approx 5.233\gamma^{-0.4211} - 0.7525 \tag{23}$$

From Equation (21), increasing R'_d and decreasing R_e affects the reduction in the undershoot voltage. For simplicity and convenience in the selection of the additional series and tail-time resistances, some simulations with various undershoot rates (from 30% to 80%) are performed and illustrated in Figure 9. The relation of R'_d and R_e associated with the undershoot rate is found here. The appropriate resistances (R'_d and R_e) can be selected by Equations (24)–(26), with the factors of (a) and (b) located in the shaded area in Figure 9, in which the undershoot rate is lower than 50% as the waveform requirement. The increase in the parallel resistance (R_p) affects the reduction in loss in the system and increases the undershoot rate. Moreover, the increase in (b) results in an increase in the series resistance (R'_d), affecting an increase in loss in the system, and a reduction in the undershoot rate.

$$Z = \sqrt{(L_d + L_L)/C_s} \tag{24}$$

$$R'_d = aZ \tag{25}$$

$$R_p = bZ \tag{26}$$
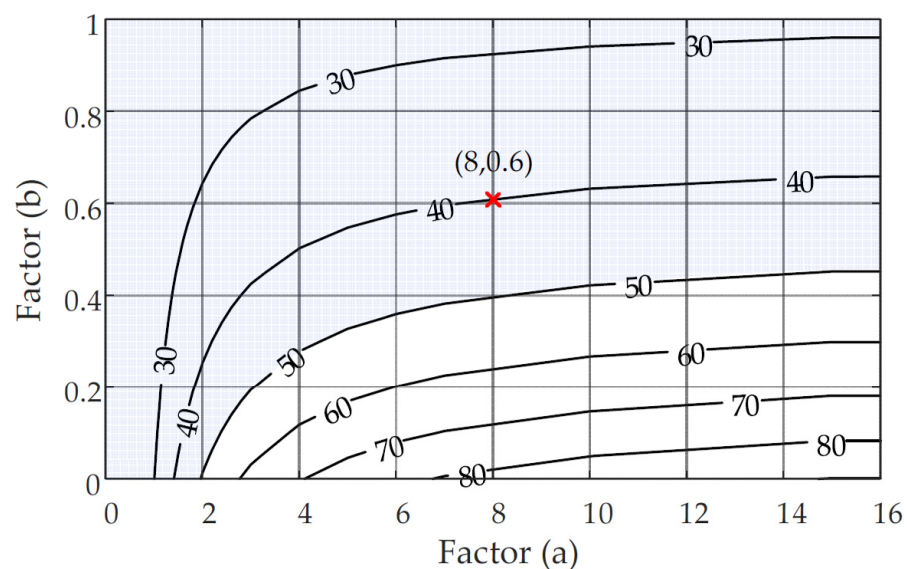
Figure 9. Undershoot rate in % with the relation of factors of *a* and *b*.

If there are many resistors available, using either the additional resistor or the tail-time resistor enables control of an undershoot rate of about 40%. R'_d and R_e can be

approximated by Equations (27) and (28), respectively. However, using both R'_d and R_e is also an alternative choice to control the undershoot voltage.

$$R'_d \approx 0.75\sqrt{(L_d + L_L)/C_s} \tag{27}$$

$$R_e \approx 1.5\sqrt{(L_d + L_L)/C_s} \tag{28}$$

3. Verification of Proposed Approach

Simulations and experiments were performed and compared to demonstrate the validity of the proposed design approach. Table 2 shows the compared circuit parameters of winding loads, and the designed circuit parameters in Cases 1 to 5, of which load inductances are in the range from 0.4 mH to 4 mH. In these simulation cases, and for the purpose of comparison of the circuit voltage efficiencies, the charging voltages were set to be one per unit. In Cases 1, 2, and 3, only the additional parallel resistor (R_p) was employed to control the undershoot rate. In Case 4, only the additional series resistor (R'_d) was employed to control the undershoot rate. In Case 5, with the factor *a* of 8 and *b* of 0.6 marked in Figure 9, both R_p and R'_d were employed to control the undershoot rate. The examples of the generated impulse voltage waveforms by the proposed approach are presented in Figures 10 and 11. The waveform parameters, i.e., the voltage efficiency, the overshoot rate, the undershoot rate, T_1 and T_2, are evaluated by the procedures recommended by the standard [15]. It is noticed that in Cases 2, 4, and 5, with the same load, using either R'_d or R_e, as well as using both R'_d and R_e for controlling the undershoot voltage in the proposed approach, provides almost the same waveform parameters. All waveform parameters in Cases 1 to 5 are within the tolerances provided by the standards [2,4,5]. Using the proposed approach, the lower the load inductance is, the higher the charging capacitance and the voltage efficiency are.

Table 2. Circuit component parameters, and the generated waveform parameters, in the considered cases.

Circuit and Time Parameters	Case 1	Case 2	Case 3	Case 4	Case 5
L_L	4.0 mH	1.0 mH	0.4 mH	1.0 mH	1.0 mH
C_b	2.0 nF	4.0 nF	8.5 nF	4.0 nF	4.0 nF
C_s	1.0 μF	4.0 μF	10.0 μF	4.0 μF	4.0 μF
R_d	200 Ω	100 Ω	50 Ω	100 Ω	100 Ω
L_d	400 μH	200 μH	100 μH	200 μH	200 μH
R_p	980 Ω	320 Ω	135 Ω	320 Ω	320 Ω
R_e	100 Ω	26 Ω	11 Ω	-	140 Ω
R'_d	-	-	-	13 Ω	10 Ω
Voltage efficiency	93.25%	85.19%	81.84%	85.44%	85.19%
Overshoot rate (<5%)	0.00%	−0.57%	−0.67%	−0.93%	−0.57%
Undershoot rate (<50%)	38.37%	39.07%	40.10%	39.27%	40.90%
T_1 (0.84 μs–1.56 μs)	1.07 μs	1.00 μs	1.02 μs	1.01 μs	1.01 μs
T_2 (40 μs–60 μs)	40.5 μs	42.8 μs	44.4 μs	42.9 μs	42.6 μs
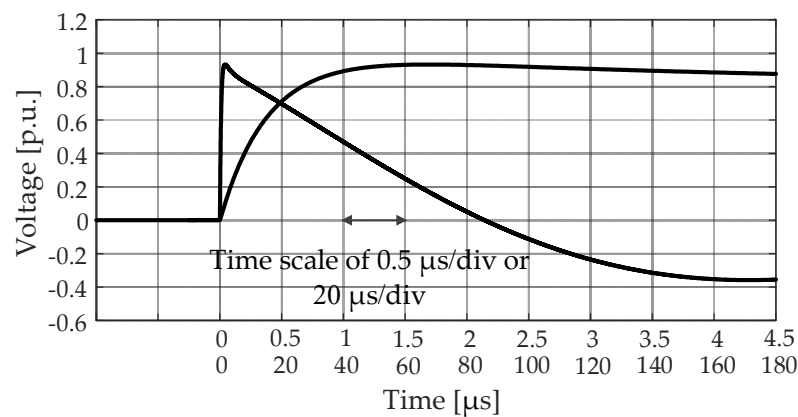
Figure 10. Generated waveform of Case 1 by the proposed approach.
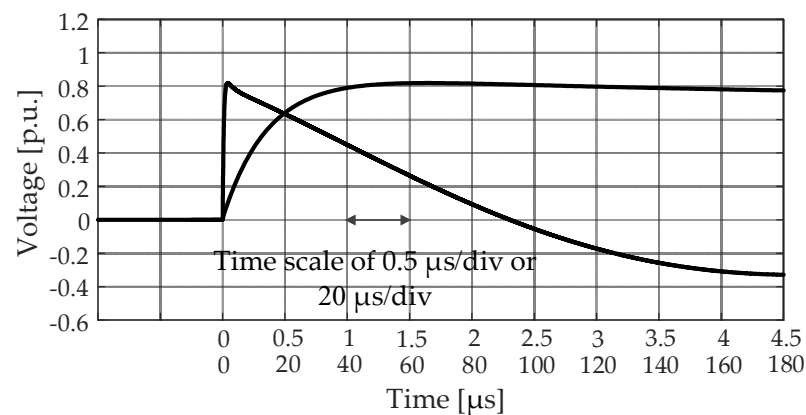
Figure 11. Generated waveform of Case 3 by the proposed approach.

The final case (Case 6) is the only case in which simulation and experimental results are compared. In this case, the low voltage inductor used in a harmonic filter system was employed as a load under tests. The load inductance (L_L) is 2.013 mH. In the experiment, the charging voltage was set to be 6.5 kV for obtaining the 6 kV peak voltage. Capacitors (1 nF voltage divider and 3 nF additional capacitor) with a total capacitance of 4 nF were connected with the test object. With the proposed approach, the selected circuit parameters of R_d, L_d, R_p, and R_e are 100 Ω, 200 μH, 500 Ω, and 50 Ω, respectively. Using these circuit parameters, the comparisons of the experiments, and simulations of the generated waveforms and waveform parameters, are presented in Figure 12 and Table 3. It was found that the simulation and experimental waveforms were in good agreement.
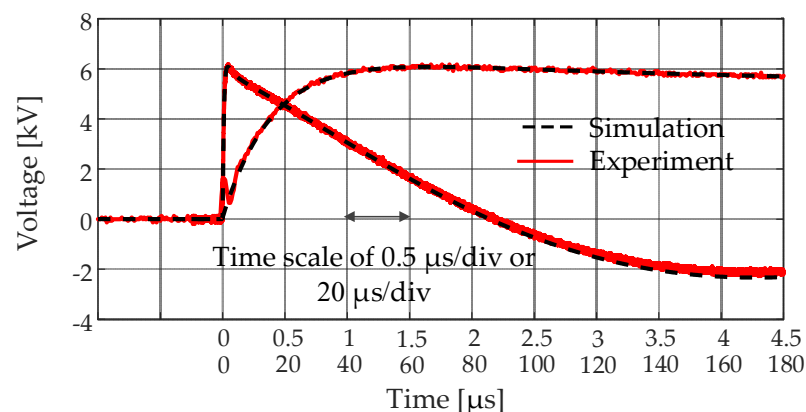
Figure 12. Comparison of the simulation and experimental waveforms in Case 6.

Table 3. Circuit and waveform parameters of the generated waveforms in the example cases.

Case	Voltage Efficiency	Overshoot Rate	Undershoot Rate	T_1 (µs)	T_2 (µs)
Simulation	93.45%	+0.17%	38.36%	1.07	40.4
Experiment	93.43%	+0.97%	35.21%	1.07	40.8

4. Conclusions

In this paper, the problems in the waveform adjustment of the lightning impulse voltage tests on low-inductance loads, i.e., the windings of transformers and reactors, have been presented. When dealing with a low-inductance load, the limitations of employing Glaninger's circuit with Feser's parameter selection approach have been recognized and explored. Glaninger's circuit has been extended to generate an accurate impulse voltage waveform according to the standard requirement. An additional series resistance (R'_d) is added to the branch, where the additional inductor (L_d) is placed in Glaninger's circuit. With this additional series resistance (R'_d), a proper selection procedure for the components in the circuit has been reviewed and refined instead of using Feser's suggestion. The advantages of the proposed method over the conventional approach are that the proposed impulse voltage generation circuits can function well with the charging capacitance up to 10 µF, and with the maximum inductance-load (the lowest inductance) of 400 µH, and there is no need of the further adjustment of the circuit components to obtain the waveform according to the standard requirements. Additionally, using the designed components, the circuit provided the impulse voltage waveform with low distortion, with an efficiency higher than 80%, and with an undershoot voltage of 40%.

References

1. Kuffel, E.; Zaengl, W.S.; Kuffel, J. *High Voltage Engineering: Fundamentals*, 2nd ed.; Newnes: Oxford, UK, 2000.
2. *High-Voltage Test Techniques. Part 1: General Definitions and Test Requirements*, 3rd ed.; IEC 60060-1; IEC: Geneva, Switzerland, 2010.
3. *IEEE Standard for High-Voltage Testing Techniques*; IEEE Standard 4TM-2013; IEEE: Piscataway, NJ, USA, 2013.
4. *Power Transformer. Part 1: General*, 3rd ed.; IEC 60076-1; IEC: Geneva, Switzerland, 2011.
5. *Power Transformer. Part 3: Insulation Level, Dielectric Tests and External Clearances in Air*, 3rd ed.; IEC 60076-3; IEC: Geneva, Switzerland, 2013.
6. *Power Transformer. Part 4: Guide to the Lightning Impulse and Switching Impulse Testing—Power Transformer and Reactors*, 1st ed.; IEC 60076-4; IEC: Geneva, Switzerland, 2002.
7. Karthikeyan, B.; Rajesh, R.; Balasubramanian, M.; Saravanan, S. Experimental investigations on IEC suggested methods for improving waveshape during impulse voltage testing. In Proceedings of the 2006 IEEE 8th International Conference on Properties & Applications of Dielectric Materials, Bali, Indonesia, 26–30 June 2006.
8. Glaninger, P. Impulse testing of low inductance electrical equipment. In Proceedings of the 2nd International Symposium on High Voltage Technology, Zurich, Switzerland, 9–13 September 1975; pp. 140–144.

9. Schrader, W.; Schufft, W. Impulse voltage test of power transformers. In Proceedings of the Workshop 2000, Alexandria, VA, USA, 13–14 September 2000.
10. Tuethong, P.; Kitwattana, K.; Yutthagowith, P.; Kunakorn, A. An algorithm for circuit parameter Identification in lightning Impulse voltage generation for low-inductance loads. *Energies* **2020**, *13*, 3913. [CrossRef]
11. Mirzaei, H. A Simple Fast and Accurate Simulation Method for Power Transformer Lightning Impulse Test. *IEEE Trans. Power Deliv.* **2019**, *34*, 1151–1160. [CrossRef]
12. Mirzaei, H.; Bayat, F.; Miralikhani, K. A Semi-Analytic Approach for Determining Marx Generator Optimum Set-up during Power Transformers Factory Test. *IEEE Trans. Power Deliv.* **2021**, *36*, 10–18. [CrossRef]
13. Feser, K. Circuit Design of Impulse Generators for the Lightning Impulse Voltage Testing of Transformers. Bull. SEV/VSE Bd 1978. Available online: www.haefely.com (accessed on 15 November 2019).
14. Yutthagowith, P.; Tuethong, P.; Pattanadech, N. Effective circuit parameter determination in lightning impulse voltage tests of air core inductors. In Proceedings of the 12th IET International Conference on AC and DC Power Transmission, Beijing, China, 28–29 May 2016.
15. *Instruments and Software Used for Measurement in High-Voltage and High Current Tests. Part 2: Requirements for Software for Tests with Impulse Voltages and Currents*, 2nd ed.; IEC 61083-2; IEC: Geneva, Switzerland, 2013.